FBG Head Size Influence on Localized On-chip Thermal Measurement in IGBT Power Modules

DOI:
10.1109/JSEN.2022.3210708

Document Version
Accepted author manuscript

Citation for published version (APA):
Durovic, S., Barnes, M., Vilchis-Rodriguez, D., Chen, S., Mckeever, P. M., & Jia, C. (2022). FBG Head Size Influence on Localized On-chip Thermal Measurement in IGBT Power Modules. *IEEE Sensors Journal*, *22*(22), 21684 - 21693. https://doi.org/10.1109/JSEN.2022.3210708

Published in:
IEEE Sensors Journal

FBG Head Size Influence on Localized On-chip Thermal Measurement in IGBT Power Modules

Shiying Chen, *IEEE Student Member*, Damian Vilchis-Rodriguez, *IEEE Member,* Siniša Djurović, *IEEE Member,* Mike Barnes, *IEEE Senior Member*, Paul McKeever, Chunjiang Jia

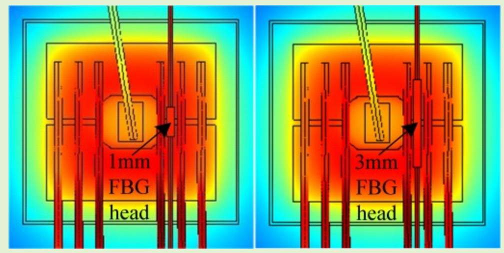

***Abstract*—This paper studies the influence of Fiber Bragg Grating (FBG) head length on insulated gate bipolar transistor (IGBT) direct on-chip thermal sensing performance of FBG sensors. To this end the surface of a commercial IGBT chip is thermally simulated and experimentally characterized. Uniform FBG sensors with three head sizes are then tested in two promising thermal sensing locations. The study has found that the large thermal gradients in this application create an additional constraint when using longer head lengths. A distortion in the reflected spectrum of the 5 mm FBG sensor is used to illustrate the underlying physical effect which causes this limitation for IGBT junction temperature measurement. This additionally affects the length of head sizes providing accurate temperature readings of the IGBT surface hotspots, and significantly this limit is location dependent in a given IGBT geometry.**

***Index Terms*—IGBT, junction temperature, FBG sensor, FBG head size, thermal distribution, on-chip thermal sensing**

I. Introduction

The insulated gate bipolar transistor (IGBT) is a key enabler of the modern power industry, with applications ranging from electric vehicles to renewables and their grid integration. Optimal exploitation of IGBTs will be crucial for facilitating our transition to zero carbon power and energy systems. One of the key bottlenecks to better utilization of IGBT power modules is the current inability to reliably sense and monitor the critical in-service thermal conditions of the device, namely the highest temperature of its junction region. Development of methods for direct, on-chip thermal sensing to monitor IGBT junction temperature is therefore attracting increased research interest.

The methods to acquire the IGBT junction temperature are generally classified into three categories: estimation based on temperature sensitive electrical parameters (TSEPs), estimation based on thermal circuits and FEA models, and optical technologies based contact and non-contact measurement [1] [2].

TSEPs such as the on-state voltage, the gate voltage, the gate current, etc. have been proposed to evaluate the junction temperature [3]-[5]. However, these methods allow for evaluation of the average junction temperature only and do not enable the monitoring of its maximum temperature, which is of most interest. In addition, the electrical parameters and the thermal resistance can change with the IGBT power module age [6] [7]. Hence the relationship between these electrical parameters and the junction temperature calibrated for a new IGBT can be affected by the aging process and therefore become inaccurate in an in-service device.

Thermal circuits and FEA models can provide an effective means for thermal performance analysis of IGBT modules [8] [9]. Their development however relies heavily on the availability of device design proprietary data, such as detailed material properties and geometry specifications, which are often challenging to obtain and may be unavailable in practice. This can compromise the accuracy of model predictions and complicate their usage for assessing practical device performance with a high degree of accuracy. In addition, the structural abnormalities arising from power module aging can give rise to change in thermal resistances and thermal capacitances, which can in turn yield estimation errors [7].

Thermal measurements using infrared (IR) cameras have been validated as a reliable method to acquire the surface thermal distribution of the IGBT chip [2] [10]. To facilitate accurate thermal measurement using an IR camera the chip surface usually requires application of specialized coating to increase the surface emissivity [11]. While useful in laboratory conditions, this method is impractical for use in industrial applications as it requires the module case to be removed. It also requires a clear line of sight to the thermal measurement location which can be obscured by IGBT bond wires geometry.

A limited number of embedded thermal measurement methods based on usage of FBG optic sensing technology have recently been proposed to monitor the IGBT temperature [12]-[15]. FBG sensing is a promising solution for IGBT module embedded temperature measurement due to its intrinsic features of EMI immunity, small size, multiplexing, flexibility, inherent robustness, power passivity and long lifetime [16]. The reported IGBT embedded FBG sensing methods [12]-[15] are in principle conceived with a view to the acquisition of accurate point temperatures. However, the development of these techniques is still at an early stage and requires further research. In [12] low current only was examined. The tests in [13] were performed close to ambient temperature only. In [14] the junction temperature is still evaluated using a thermal circuit model. The authors' study in [15] proposes to interface

Shiying Chen, Damian Vilchis-Rodriguez, Siniša Djurović and Mike Barnes are with the Department of Electrical and Electronic Engineering, the University of Manchester, Manchester, M13 9PL, UK (sinisa.durovic@manchester.ac.uk;)

Paul McKeever and Chungjiang Jia are with the Offshore Renewable Energy (ORE) Catapult, Newcastle upon Tyne, NE24 1LZ, UK

the FBG sensor head to chip surface using thermal paste and thus facilitate in-service measurement of localized junction temperature. Good measurement accuracy of this method is reported up to module rated operating current.

FBG sensors have been shown to have potential for in situ on-chip measurement, but further research is required to capture localized thermal conditions. This is particularly valid where the effect of the applied FBG sensing head size is concerned, as the capture of maximum temperature on the small chip surface characterized by uneven heat distribution may be affected or compromised by unsuitable head dimension. The aim of this work is to characterize the influence of sensing head length on localized temperature sensing in a commercial IGBT module and evaluate the general requirements for effective thermal point sensing. The thermal map of the examined module was first simulated using finite element analysis to characterize its surface heat distribution and inform the sensor locations of interest. A specialized test rig was then used to perform tests on the chip geometry separately fitted with three different size FBG sensors and evaluate in-situ thermal monitoring performance. Different orientation sensing on the chip surface was assessed, along with the corresponding surface temperature distribution gradients and their effect on individual sensor performance and in-situ applicability.

II. Principles of Fiber Bragg Grating Sensing

The FBG sensor is a distributed Bragg reflector imprinted within the optical fiber core. Its typical structure is shown in Fig. 1: the sensor head is a segment of several adjacent gratings in the fiber core; the fiber is made of a core surrounded by a cladding layer, which is generally protected by a coating layer. The diameter of the cylindrical glass core is in the range of 4-9 µm, and the diameters of the cladding layer and the coating layer are about 125 µm and 150 µm, respectively.

A discrete wavelength of the light propagated within the core will be reflected by the Bragg reflector and is called the Bragg wavelength λ_B. This wavelength shifts with temperature, $\Delta\lambda_B$, in a relationship that can be described as [17]:

$$\Delta\lambda_B = \lambda_B\,(\alpha + \xi)\,\Delta T \qquad (1)$$

where α is the fiber thermal expansion coefficient ($\approx 0.55 \times 10^{-6}$ /°C) and ξ is the thermo-optic coefficient (≈ 6 to 9×10^{-6} /°C) [17]. Therefore, the thermal sensitivity ($\Delta\lambda_B / \Delta T$) of a standard FBG sensor whose wavelength is ≈ 1550 nm at 25 °C is evaluated to be ≈ 10 to 14 pm/°C [18]. The relationship between temperature and wavelength of a given FBG sensor can be calibrated so that the measured value of temperature can be inferred accurately from the reflected Bragg wavelength.

III. Simulated IGBT Thermal Distribution

A Semikron SKM50GB12T4 IGBT module is used in this study, as shown in Fig. 2 (a). Its IGBT chip geometry is shown in Fig. 2 (b).

A. Model geometry

The IGBT power module has a layered structure, as shown in Fig. 3.

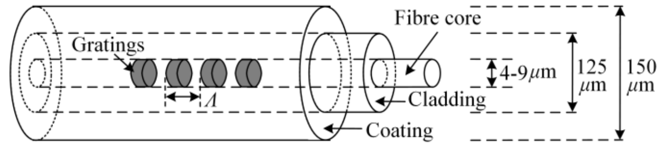

Fig. 1. Typical structure of the FBG sensor

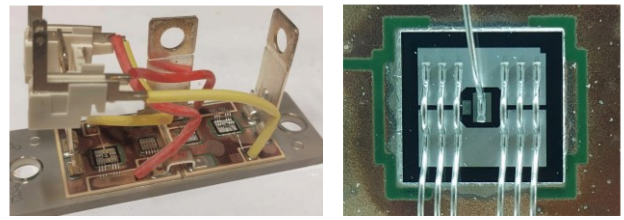

(a) (b)

Fig. 2. Test IGBT module. (a) Full view of the module. (b) IGBT chip geometry

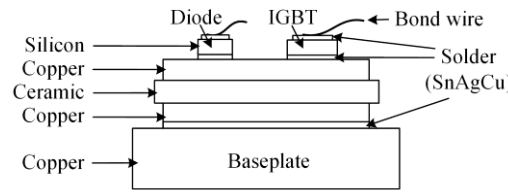

Fig. 3. The layered structure of the IGBT power module

TABLE I
IGBT Module Materials and Physical Properties

Layer name	Layer material	Thermal cond. [W/m·K]	Heat cap. [J/(kg·K)]	Density [kg/m³]	Electrical cond. [S/m]
Bond wire	Al	240	930.6	2700	3.670e7
Solder	SnAgPb	63	232.0	7370	9.100e6
IGBT die	Si	119	757.7	2329	$4.15e5T^{-1.408}$
Copper	Cu	396	392.6	8850	5.998e7
Ceramic	Al_2O_3	25	880.0	3890	1.502e-7

The thermal FEA model was constructed in COMSOL 5.5 and the geometry of each layer was measured based on cross-sectional analysis of the actual test IGBT power module [19]. COMSOL's 'Heat transfer in solids' and 'Electric Currents' physics are used in the numerical simulation. [19] provides a detailed description of the model implementation. The IGBT chip has a length of 7.2 mm and a width of 6.8 mm, while the top solder layer (silver area) has a length of 5.8 mm and a width of 5.4 mm. The constituent material of each layer is detailed in Table I [15].

The established FEA model was appropriately meshed to ensure simulation accuracy in high stress areas and reduce the numeric analysis requirements in low interest areas. Meshing details are illustrated in Fig. 4.

B. FEA thermal analysis

Due to module symmetry and to minimize computational requirements the thermal study focused on one of two IGBT chips contained in the test module (left chip in Fig. 4). The rated current of the test IGBT module is 50 A. Generally, the IGBT is controlled by PWM signals so that current only flows through the chip when it is switched on. For analysis purposes chip operation with a PWM control signal duty cycle of 50% and a nominal current amplitude of 50 A was investigated in this section. The chip's steady-state thermal distribution in this condition was obtained from the FEA model by applying an equivalent RMS current to terminal T1 while setting T3 to ground. The background temperature was set to 22.0 °C and the heat transfer coefficient of the baseplate bottom surface to 3000 W/(m^2 K). The obtained thermal distribution is shown in Fig. 5(a). The hot spot is located in the vicinity of the bond wires. To enable exploration of the chip surface temperature the bond wires were removed from view, shown in Fig. 5 (b), where the isotherms are marked: the hottest surface areas are those with the highest current density, found around the soldering connections of the bond wires. The test IGBT's gate is in the chip center, resulting in a quasi-radial temperature distribution on the chip surface. The simulation results indicate a chip surface temperature variation range of ≈ 23 °C.

To further illustrate the chip surface temperature distribution in different orientations and provide insights related to sensor positioning, two auxiliary lines are drawn in Fig. 5 (b). Fig. 6 shows the predicted temperature distribution profile along line 1 (left to right) and line 2 (upper to lower side) in the solder layer.

The highest temperature along the horizontal line 1 thermal gradient is around its center point. In contrast, two temperature peaks are found along the vertical line 2, where the line center location does not constitute the thermal hot spot; the two hottest areas are in the vicinity of bond wire solder connections. This

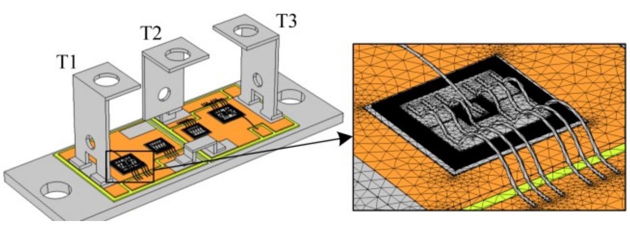

Fig. 4. The power module FEA model and IGBT mesh detail

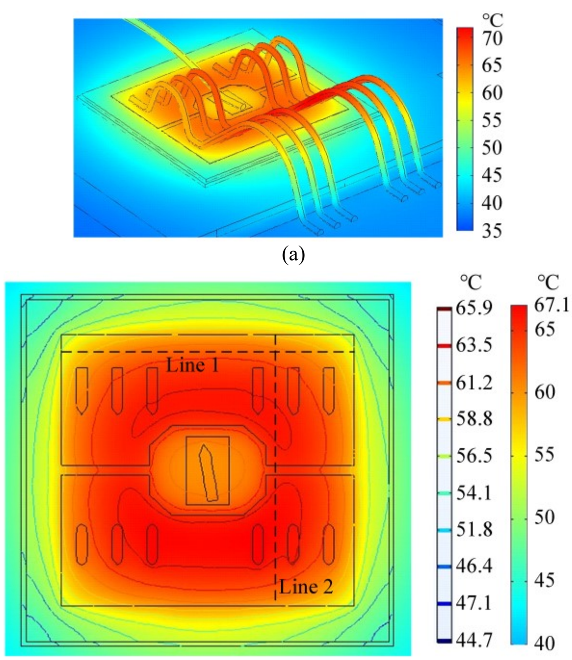

Fig. 5. FEA simulated thermal distribution of the IGBT chip. (a) IGBT chip with bond wires. (b) IGBT chip without bond wires.

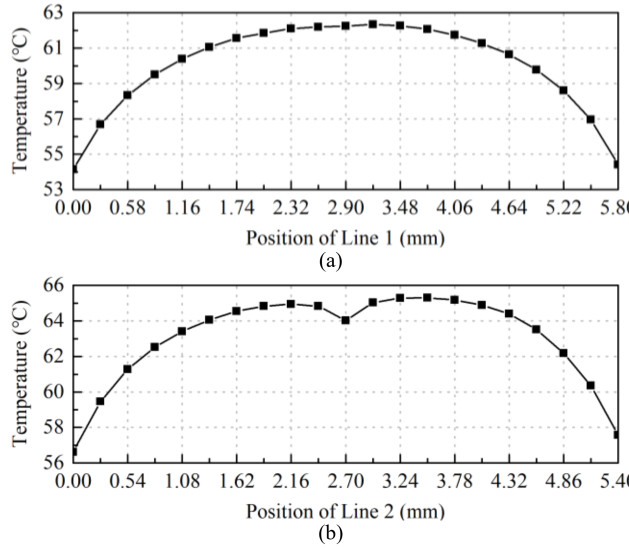

Fig. 6. FEA simulated temperature distribution along: (a) Line 1. (b) Line 2.

illustrates the FBG head placement challenges related to observation of localized surface thermal hotspots in a typical commercial IGBT geometry. It is also interesting to note the relatively considerable range (≈ 8°C) of Fig. 6 temperature profiles. The practical implications of such variation on the FBG temperature measurement are examined in the following sections.

IV. Test System and Temperature Distribution Characterisation

A. The test rig

A purpose designed test rig was built to enable FBG sensing performance evaluation in energized test IGBT modules, instrumented with different head size FBGs. The rig details are shown in Fig. 7 [15]. A 5kW DC supply, rated at a maximum of 50 A/100 V is used to power the test device. The load is rated at 2/3 Ω and 7.5 kW. An MSP430 microcontroller is used to generate the PWM control signals. Si8271 gate drivers are used. Table II shows the key parameters of the used equipment.

Two Semikron SKM50GB12T4 IGBT modules were fitted on forced air-cooled heat sinks. A 0.5 mm thick 6 W/(m·K) thermal conductivity thermal pad was placed between modules and their sinks to ensure good thermal conduction. While each module contains two IGBT chips, only one chip per module was connected in the circuit. The two chips were connected in parallel and controlled using PWM signals, as detailed in [15]. The two chip control signals were complementary and applied with a 50% duty cycle. One of the chips was the device under test, i.e. is a specialized module installed with an FBG sensor. The FBG sensor is monitored using a commercial interrogator (SmartScan04). A Fluke Ti10 thermal camera was used for chip surface temperature distribution measurement. The camera was placed above the test chip, whose surface was appropriately coated to increase emissivity and ensure reliable measurement.

B. Test IGBT surface temperature distribution

To characterize the chip's in-service surface temperature distribution, with a view to identifying sensor locations of interest, the test chip was driven at the nominal current of 50 A and 1 kHz PWM frequency and its surface thermal images taken at thermal equilibrium. The ambient temperature was ≈22.8°C. The obtained thermal image is shown in Fig. 8, including the position of line 1. The observed hotspot locations agree with those predicted by the simulations in section III.

Fig. 9 shows the measured temperature profile of line 1 (shown in black). The gate bond wire obstructs the area around the centre of line 1, resulting in a low temperature reading. The actual temperature in this region is higher, as illustrated in simulation results (Fig. 6a), but cannot however be directly measured with the thermal camera. The unobstructed measurements area reports similar temperatures to simulated results, thus further verifying their validity. To enable understanding of the possible thermal gradient in the obstructed area the line 1 thermal measurements obtained with clear line of sight were curve fitted (4^{th} order fit) to provide an indicative profile of the full line 1 thermal profile (in red in Fig. 9).

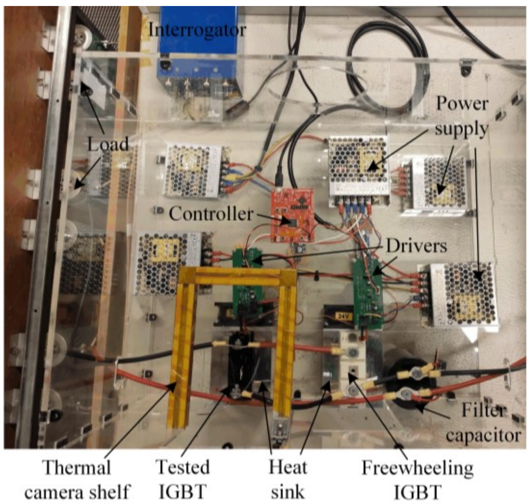

Fig. 7. The test rig

TABLE II
KEY SPECIFICATION OF THE EQUIPMENT USED FOR EXPERIMENTS

Equipment	Type	Details
Main power supply	Sorensen SGI	Rated 50A/100V/5kW
Auxiliary power supply	Switching Power Supply	Rated 2.4A/15V/35W
IGBT	SKM50GB12T4	Rated 50A/1200V
Load	Braking resistance	0.67Ω/ Rated 9kW
Controller	MSP430 F5529	16-Bit RISC Architecture, up to 25-MHz System Clock
Driver	Si8271 based	Max 60 ns propagation delay
Thermal camera	Fluke Ti10	Accuracy ±5 °C or 5 %
		Thermal Sensitivity (NETD) ≤0.2 °C at 30 °C
		Temperature Range -20 °C to +250 °C
Interrogator	SmartScan04	Repeatability < 1 pm
		Max. scan freq. 2. kHz
Capacitor	Aluminum electrolytic	4700μF/60V
Heat sink	Forced air cooling	max. air flow 80 m^3/h

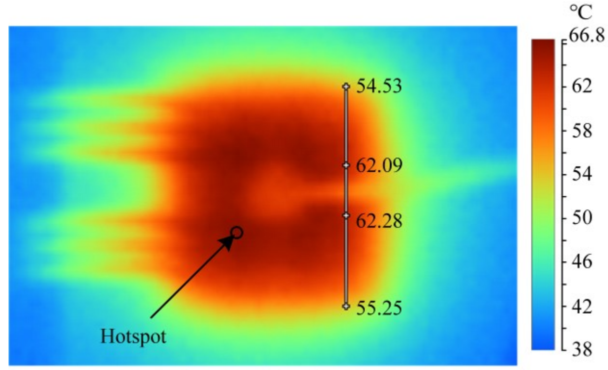

Fig. 8. IGBT surface thermal image at 50 A DC current

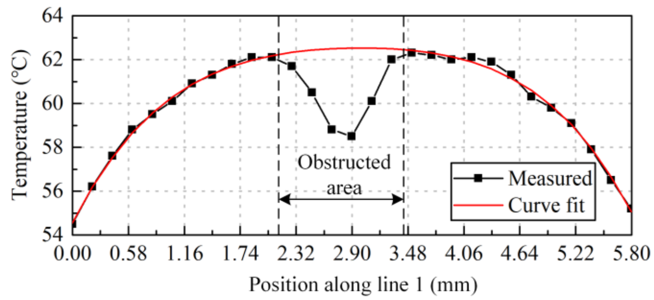

Fig. 9. Surface temperature distribution along line 1.

V. DIFFERENT HEAD SIZE FBG SENSOR PERFORMANCE ANALYSIS - EXPERIMENTAL STUDY

The sensor head size influence on thermal sensing performance was tested for a range of current operating points on the test IGBT using the head interfacing method presented in [15]: once the sensor is positioned in the desired area on the IGBT surface a high conductivity thermal paste is used to fill the gap between the fiber and the chip surface and provide improved heat conduction. The fiber termination is loosely inserted into a Teflon capillary to retain position. The other fiber end is fixed using glue to ensure stable positioning.

A. IGBT-FBG location 1 test cases

1 mm, 3 mm and 5 mm FBG head lengths were assessed in experiments. Fig. 10 illustrates the 1mm sensor instrumented IGBT chip: the FBG head location is marked red. The 3 and 5 mm sensors are situated in the same position and direction. The mid points of all three considered head lengths are kept in identical location in tests, to provide consistency of comparison and assessment of length effects. The shaded sections of the IGBT bond wires in Fig. 10 represent the solder areas.

Fig. 11 illustrates the respective simulated thermal excitation profiles that the three examined FBG lenghts are exposed to in-situ. This clearly shows that the sensing heads are exposed to non-uniform thermal excitation in this application, the scale of which is effectively defined by their length: the range of in-situ thermal excitation variation for the 1 mm, 3 mm, and 5 mm is predicted as ≈ 0.15 °C, ≈ 1.3 °C, and ≈ 5.0 °C, respectively. A longer FBG head evidently results in a wider range thermal excitation imposed on the sensor. For the assessed IGBT geometry the thermal gradient that the 5 mm FBG sensor is expected to experience exceeds 2 °C/mm.

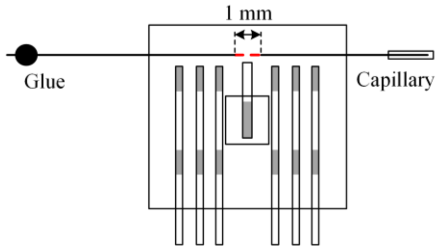

Fig. 10. 1 mm FBG positioning for location 1.

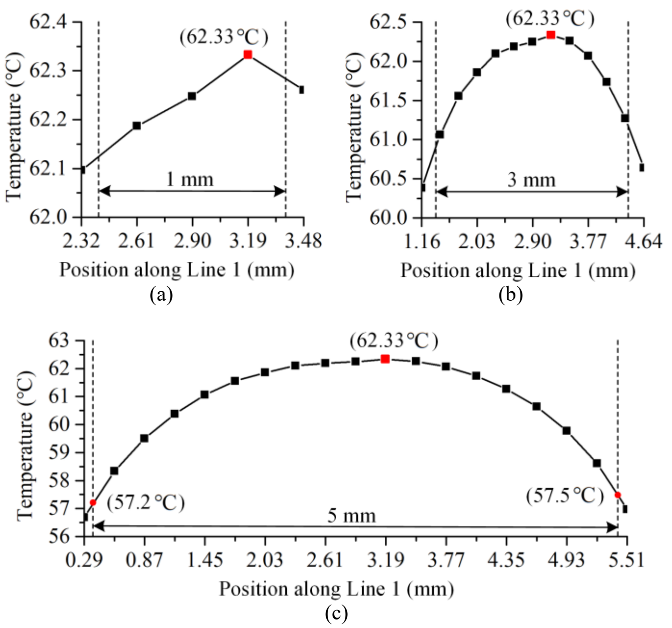

Fig. 11. Thermal excitation profile at location 1 for: (a) 1 mm FBG sensor. (b) 3 mm FBG sensor. (c) 5 mm FBG sensor.

B. IGBT-FBG location 1 test results

The three IGBT modules instrumented with different length FBG sensors were individually operated and the reflected wavelengths recorded. These were then translated to temperature using the calibrated wavelength to temperature (λ-T) relationship. Tests were performed at different constant current levels and switching frequencies; a constant current level varying from 10A to the rated 50 A in steps of 10 A was applied to provide a representative range of in-service thermal conditions. The PWM switching frequencies of 10 Hz, 100 Hz and 1 kHz were applied in all these cases. Measurements were taken once thermal equilibrium was reached for each assessed current level.

The average measured chip temperatures, T_j, of all three cases are shown in Table III and Table IV. To eliminate interference from the inevitable fluctuation in ambient temperature between tests, the measured temperature minus the measured ambient temperature, T_j - T_a, as shown in Table V and Table VI, is used for comparison.

The T_j - T_a temperature increase for the three FBG head size cases is compared in Figs. 12 to 14 at 1 kHz, 100 Hz, and 10 Hz switching frequency, respectively. The temperature sensed by the three sensor sizes in identical operating conditions is seen to differ by up to ≈ 6.0 °C.

The measurements are seen to manifest consistent trends across different switching frequencies. The 1 mm sensor constantly reported the highest reading and the 5 mm sensor the minimum temperature. The 3 mm sensor readings were higher than those of the 5 mm sensor and lower than the readings of the 1 mm sensor. For the 50 A tests, the temperature measurement difference between the three FBG sizes is at maximum. The readings of the 3 mm FBG sensor show ≈ 1.6 °C to1.9 °C lower temperature than those of the 1 mm FBG sensor, while the 5 mm FBG sensor shows ≈ 5.2 °C to 6.0 °C lower temperature than the 1 mm FBG sensor.

TABLE III
MEASUREMENTS AT LOCATION 1, 1 KHZ AND 100 HZ (°C)

Switching frequency	1 kHz			100 Hz		
FBG sensor head length	1 mm	3 mm	5 mm	1 mm	3 mm	5 mm
10 A	27.0	27.0	26.9	26.6	27.1	27.0
20 A	32.4	32.5	31.1	32.8	32.7	30.8
30 A	39.6	39.3	37.7	40.3	39.8	37.7
40 A	49.1	48.8	45.8	49.9	49.7	46.3
50 A	60.1	59.8	55.6	62.0	61.2	56.1

TABLE IV
MEASUREMENTS AT LOCATION 1, 10 HZ (°C)

Switching frequency	10 Hz		
FBG sensor head length	1 mm	3 mm	5 mm
10 A	26.9	27.3	26.7
20 A	32.6	32.8	30.2
30 A	40.4	39.7	37.4
40 A	50.1	49.7	46.1
50 A	62.4	61.2	55.9

TABLE V
T_J - T_A AT LOCATION 1, 1 KHZ AND 100 HZ (°C)

Switching frequency	1 kHz			100 Hz		
FBG sensor head length	1 mm	3 mm	5 mm	1 mm	3 mm	5 mm
10 A	3.6	3.3	3.3	3.5	3.2	3.4
20 A	9.0	7.8	7.3	9.3	7.9	7.3
30 A	16.2	14.4	13.9	16.7	14.9	14.0
40 A	25.5	23.9	21.6	26.2	24.8	22.5
50 A	36.6	35.0	31.4	38.1	36.2	32.1

TABLE VI
T_J - T_A AT LOCATION 1, 10 HZ (°C)

Switching frequency	10 Hz		
FBG sensor head length	1 mm	3 mm	5 mm
10 A	3.7	2.5	2.4
20 A	9.2	7.9	7.4
30 A	16.7	14.8	12.5
40 A	26.2	24.7	22.8
50 A	38.2	36.6	32.5

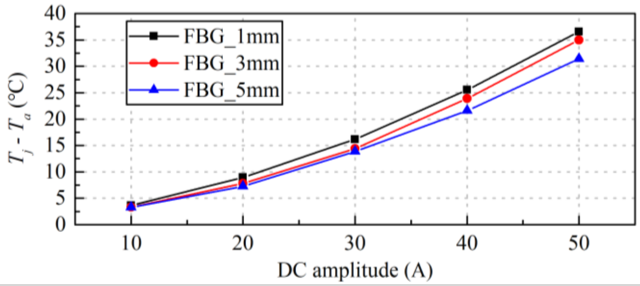

Fig. 12. Measurements of location 1 at 1 kHz switching frequency

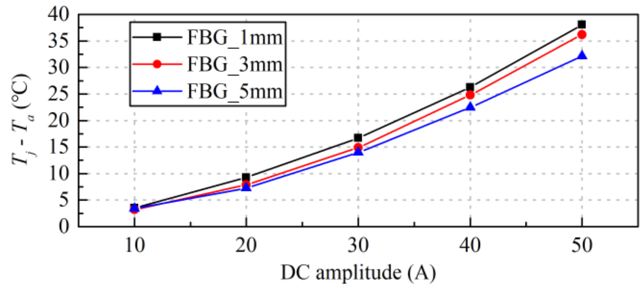

Fig. 13. Measurements of location 1 at 100 Hz switching frequency

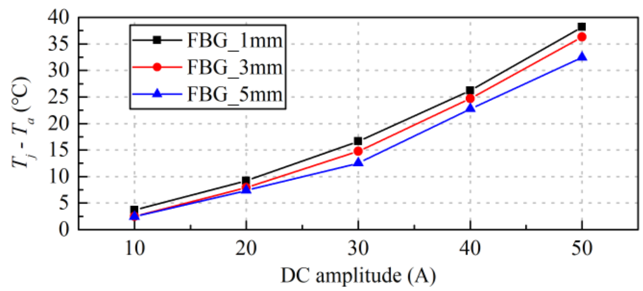

Fig. 14. Measurements of location 1 at 10 Hz switching frequency.

C. IGBT-FBG cases for location 2

The sensing performance of three different length sensors was separately tested in location 2 depicted by Line 2 in Fig. 5. To this end 1mm, 3 mm, and 5 mm sensors were installed in location 2, and their midpoints centred in the same position in tests for consistency of comparison. An illustration of a 3 mm instrumented chip is shown in Fig. 15, with the sensor head shown in red. Fig. 16 shows the non-uniform thermal excitation profiles that the three FBG sensors are exposed to in-situ.

D. IGBT-FBG location 2 test results

The tests were performed consistently to those in section V. B with 10 A to 50 A constant current applied at a time in steps of 10 A, and identical switching frequencies considered. The obtained measurements are listed in Tables VII and VIII. The measured temperature minus the measured ambient temperature, T_j - T_a, are shown in Figs. 17 to 19 and listed for clarity in Tables IX and X. The difference in sensed temperature between sensors in this location at identical conditions was measured to reach up to ≈ 4.0 °C.

The 5 mm sensor reported the lowest temperature readings, while the 3 mm sensor sensed the highest temperature. This is driven by the temperature distribution along line 2 and the respective sensor head length, as illustrated in Fig. 16. A given head length in combination with the corresponding spans of the line 2 profile thermal variation will determine the thermal excitation variation imposed on the in-situ sensor. Along line 2, thermal hotspots are exhibited in bond wire solder areas with a relatively lower temperature present between these, where the sensing head is centred in tests. This means that the 3 mm FBG will span the line 2 thermal variation area including the two thermal hotspots, and would thus generally be expected to report the highest thermal reading. The 1 mm sensor is located between the two hotspot areas hence the measured temperature is lower. Finally, the 5 mm sensor length covers a line 2 span with thermal variation of ≈ 6.5 °C below hotspot temperature and thus reports the lowest thermal readings.

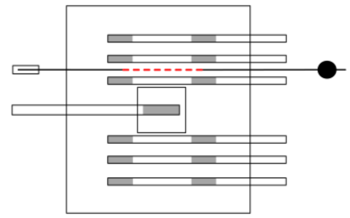

Fig. 15. The 3 mm IGBT-FBG case for location 2.

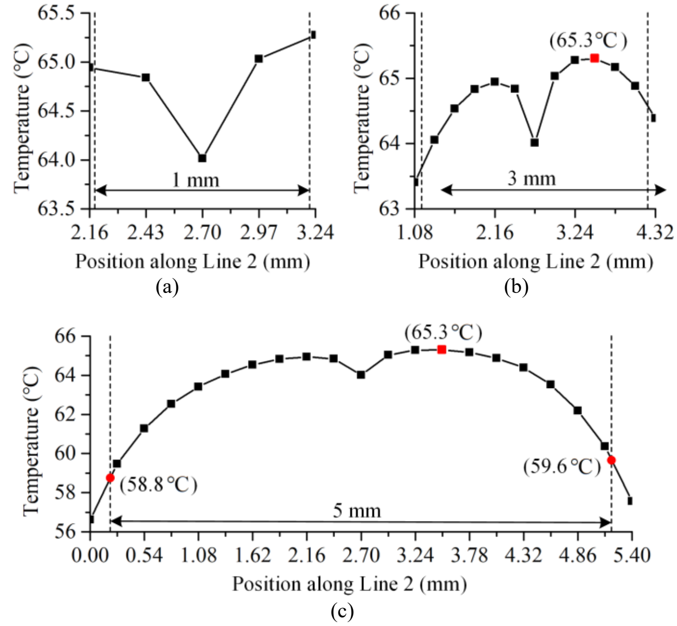

Fig. 16. FBG sensors thermal excitation profiles at location 2 for: (a) 1 mm FBG sensor. (b) 3 mm FBG sensor. (c) 5 mm FBG sensor.

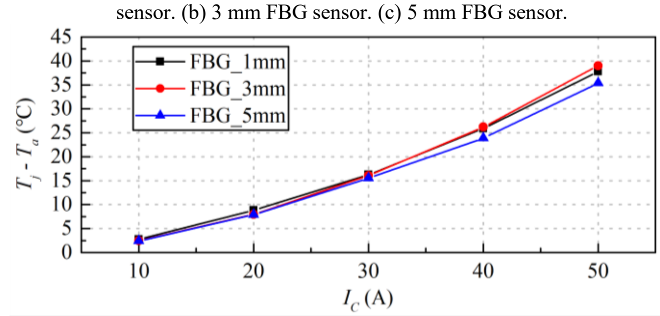

Fig. 17. Measurements of location 2 at 1 kHz switching frequency

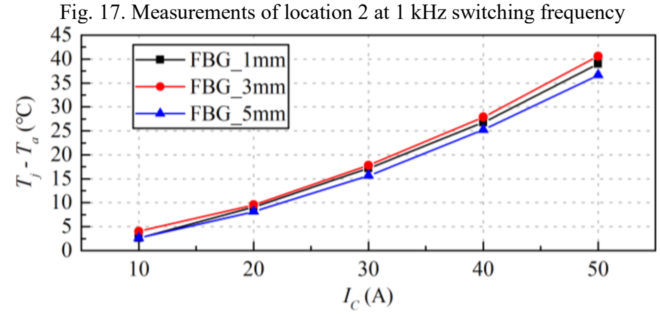

Fig. 18. Measurements of location 2 at 100 Hz switching frequency

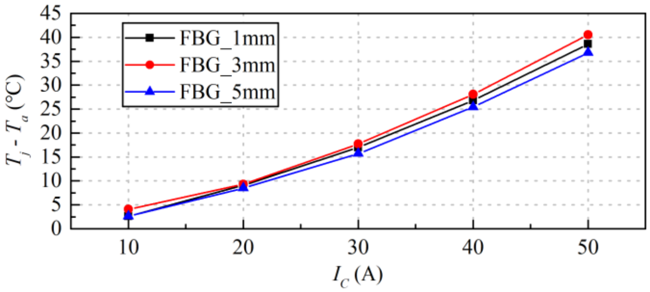

Fig. 19. Measurements of location 2 at 10 Hz switching frequency

TABLE VII
MEASUREMENTS AT LOCATION 2, 1 KHZ AND 100 HZ (℃)

Switching frequency	1 kHz			100 Hz		
FBG sensor head length	1 mm	3 mm	5 mm	1 mm	3 mm	5 mm
10 A	28.0	28.1	28.7	28.4	28.6	29.0
20 A	34.6	33.9	34.8	35.1	34.3	35.2
30 A	42.8	42.3	42.4	43.2	43.1	42.9
40 A	52.5	52.8	51.6	53.1	53.4	52.2
50 A	64.2	64.7	62.7	64.9	65.7	63.7

TABLE VIII
MEASUREMENTS AT LOCATION 2, 10 HZ (℃)

Switching frequency	10 Hz		
FBG sensor head length	1 mm	3 mm	5 mm
10 A	29.0	28.7	29.3
20 A	35.6	34.5	35.5
30 A	43.9	43.3	43.1
40 A	53.8	53.6	53.5
50 A	65.9	66.1	64.4

TABLE IX
T_J - T_A AT LOCATION 2, 1 KHZ AND 100 HZ (℃)

Switching frequency	1 kHz			100 Hz		
FBG sensor head length	1 mm	3 mm	5 mm	1 mm	3 mm	5 mm
10 A	2.7	2.5	2.4	2.6	4.0	2.6
20 A	8.8	8.0	7.9	9.1	9.5	8.2
30 A	16.2	16.1	15.5	17.2	17.8	15.6
40 A	25.9	26.2	23.9	26.7	27.9	25.2
50 A	37.8	39.0	35.4	39.0	40.6	36.6

TABLE X
T_J - T_A AT LOCATION 2, 10 HZ (℃)

Switching frequency	10 Hz		
FBG sensor head length	1 mm	3 mm	5 mm
10 A	2.6	4.1	2.6
20 A	9.1	9.3	8.5
30 A	17.0	17.7	15.7
40 A	26.8	28.1	25.4
50 A	38.6	40.5	36.8

E. Experimental results discussion

The IGBT chip surface temperature distribution is non-uniform and can exhibit considerable thermal gradients. The resulting temperature distribution profiles along lines of different orientation and length on chip surface therefore vary in form significantly. As the on-chip FBG sensor application is inherently made along a narrow surface line length, this has important measurement implications in that the sensor can generally be expected to be exposed to non-uniform thermal excitation in-situ: the extent of excitation non-uniformity is determined by the orientation specific surface temperature distribution profile characteristics and the sensing head length. Furthermore, it has been shown that for uniform FBGs subjected to pronounced thermal gradients a considerable error in measurement can occur [20]. Hence, a careful choice of FBG sensor head length becomes important.

For the analysed IGBT geometry, based on the obtained results it was found that for location 1 profile, containing a single localised thermal hotspot in the profile centre, the 1 mm FBG reported the thermal readings closest to those predicted by the FEA simulation. The longer 3 and 5 mm FBG sensors reported values that were ≈ 1.6 ℃ to 1.9 ℃ and ≈ 5.2 ℃ to 6.0 ℃ lower than those of the 1 mm FBG, respectively. This presents an up to 16% relative deviation from the 1 mm sensor measurement in case of the 5 mm FBG, which can constitute a prohibitive deviation margin where higher accuracy of hotspot measurement is required. In contrast, for location 2 with two relatively closely located temperature peaks, the 3 mm FBG generally reports the temperature closest to the FEA predicted hotspot. The 1 mm sensor provides slightly lower readings, reflecting the fact that the midpoint of location 2, where the sensor is located, exhibits a limited temperature drop. The 5 mm FBG measurements are ≈ 3.6 ℃ to 4.0 ℃ lower than those of the 3 mm FBG, demonstrating that a long FBG head in this orientation reports readings somewhat closer to those of shorter FBGs, as driven by the nature of the location 2 thermal profile.

The results indicate that the selection of sensing head length to achieve effective localised hot spot measurement is crucial and fundamentally defined by the interplay between the actual thermal hotspot location and the related surrounding surface temperature distribution characteristics. In general, a shorter FBG head length can intrinsically provide a more credible measurement, assuming it can be located sufficiently close to the localised hotspot being monitored, which can be challenging in practical applications. In some locations (e.g. location 2 in this study) the application of a longer FBG sensing head can provide optimal results and would enable less stringent installation requirements in terms of positioning. Very long head sizes that are comparable to chip surface dimension however are generally expected to result in the highest level of the hotspot temperature reading deviation and inaccuracy.

Finally, to provide a wider overview of FBG application for IGBT direct on-chip thermal sensing a comparison of this work with limited existing studies is summarized in Table XI.

VI. FBG REFLECTED SPECTRUM DISTORTION

Section V measurements report a sizeable deviation of the 5 mm FBG measurement in location 1. This section studies the underlying cause of this deviation when a long FBG sensor has

TABLE XI
COMPARISON OF PROPOSED WORK WITH PREVIOUSLY REPORTED WORK

Reference	Test current (A)	Temperature range (°C)	Installation position	Head Length (mm)
Reported work	10 to 50	26 to 70	chip surface	1, 3, 5
[12]	1.3	Ambient + 1.26	chip surface	/
[13]	200 to 400	19 to 26	chip surface	10
[14]	10 to 50	18 to 36	baseplate	5
[15]	30, 50	30 to 80	chip surface	3

to cope with an area with a large thermal gradient and consequently a significant non-uniformity in thermal excitation. To this end the reflected wavelengths of individual sensors are measured and compared to highlight the effect of surface temperature variation on measurement as function of head size in this application. To allow clear assessment of uneven thermal excitation the spectra reflected by the IGBT installed 1 mm, 3 mm and 5 mm FBGs were recorded in three conditions: 1) At ambient temperature; 2) In a thermal chamber at stable 50 °C; 3) On the test rig with IGBT current heating the chip to 50 °C (defined using 1 mm FBG reading). In the first two conditions, the temperature of the entire chip geometry is homogeneous with no thermal gradients present. In contrast, in a current heated IGBT, the chip surface exhibits large thermal gradients and localised temperature variation

The recorded spectra of the 1 mm FBG are shown in Fig. 20. The shape of the reflected spectrum is seen to be closely similar across the three observed excitation scenarios. This suggests that the uneven thermal excitation resulting from IGBT current flow does not detrimentally affect the 1 mm FBG head measurements, as this length is sufficiently small to avoid exposure to a large excitation temperature non-uniformity. A similar observation can be made for the measured spectra of the 3 mm FBG, Fig. 21, where reflected spectra shape is maintained across the three examined scenarios. The measured 5 mm FBG spectra in Fig. 22 however show a distortion in the reflected spectrum with presence of non-uniform thermal excitation resulting from IGBT current flow. While the spectrum shape at uniform thermal excitation (i.e. ambient and thermal chamber) is identical, the non-uniform excitation results in an alteration of the spectrum (in green in Fig. 22) and an overall reduction in reflected wavelength value. This will in turn alter the FBG and the interrogator reading of the wavelength in these conditions and result in an alteration of the actual measured value [20]. This effect causes the thermal measurement deviation observed in section V tests, as the combination of a long FBG head and a location with a pronounced thermal gradient / non-uniformity will inevitably experience this phenomenon in this application.

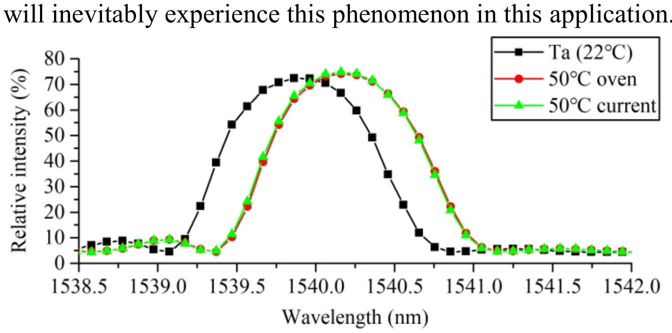

Fig. 20. Measured spectra of the 1 mm FBG sensor

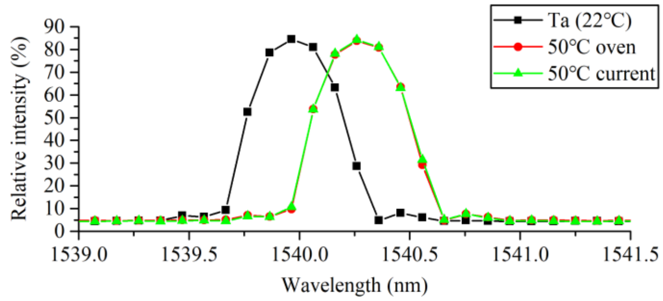

(a)
Fig. 21. Measured spectra of the 3 mm FBG sensor

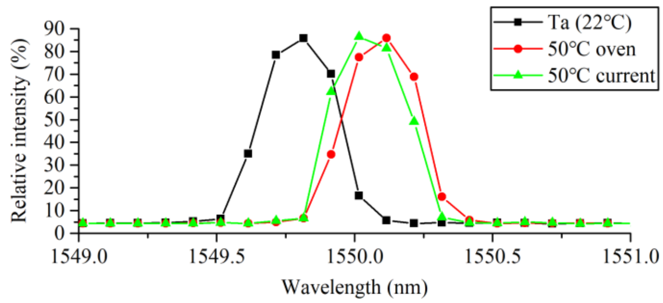

Fig. 22. Measured spectra of the 5 mm FBG sensor

VII. CONCLUSION

This paper evaluates the influence of the FBG sensor head length on the attainable performance of IGBT power module direct on-chip thermal sensing with FBG technology. The study employs a specialized test system involving a number of commercial IGBTs instrumented with different size FBG heads for thermal sensing in the modules' rated operating envelope. An IGBT FEA thermal model is also developed to provide further understanding of the chip's thermal behavior.

The experimental and model characterization of the studied IGBT show a considerable non-uniformity in the chip's surface temperature distribution, and thus in the thermal excitation of surface applied uniform FBG sensors. The selection of FBG size is crucial for reliable measurement in these conditions: the effective capture of the hotspot temperature of interest is found to be a tradeoff between the choice of FBG size and the surface temperature distribution characteristics of the hotspot location. Very short head sizes will inherently provide more accurate reading of localized IGBT surface hotspots, which are typically in a small area and can be deemed to constitute a surface point temperature with no pronounced thermal gradient. Application of short FBGs however comes at a penalty of requiring precise determination of hotspot locations and accurate placement of sensors in these, which can be challenging. Longer FBGs are able to provide reliable thermal readings in locations characterized by less severe thermal gradients; these can also provide additional advantages compared to very short FBG sensors in terms of placement and therefore installation ease. However, very long FBGs, comparable in size to the chip length were found to exhibit reflected wavelength change when subjected to pronounced non-uniform thermal excitation on the IGBT surface. This can lead to significant deviation in thermal measurement and generally renders these much less suitable for IGBT on-chip thermal sensing application, due to large thermal gradients these devices may exhibit under practical loads.

The reported study provides further understanding of the key application requirements for effective FBG sensing application for direct on-chip thermal hotspot monitoring in power electronic switches. The findings demonstrate the potential of FBG sensors for practical on-chip implementation in tests on a commercial IGBT geometry, and for enabling a much improved awareness of chip in-service thermal conditions which would be impractical to achieve using conventional thermal sensing techniques.

References

[1] M. H. M. Sathik, J. Pou, S. Prasanth, V. Muthu, R. Simanjorang and A. K. Gupta, "Comparison of IGBT junction temperature measurement and estimation methods-a review," *2017 Asian Conference on Energy, Power and Transportation Electrification (ACEPT)*, 2017, pp. 1-8.

[2] B. Wang, J. Cai, X. Du and L. Zhou, "Review of power semiconductor device reliability for power converters," in *CPSS Transactions on Power Electronics and Applications*, vol. 2, no. 2, pp. 101-117, 2017.

[3] V. Smet, F. Forest, J. J. Huselstein, A. Rashed, and F. Richardeau, "Evaluation of V_{ce} monitoring as a real-time method to estimate aging of bond wire-IGBT modules stressed by power cycling," *IEEE Trans. Ind. Electron.*, vol. 60, no. 7, pp. 2760–2770, Jul. 2013.

[4] S. Zhou, L. Zhou, and P. Sun, "Monitoring potential defects in an IGBT module based on dynamic changes of the gate current," *IEEE Trans. Power Electron.*, vol. 28, no. 3, pp. 1479–1487, Mar. 2013.

[5] M. A. Rodriguez-Blanco *et al.*, "A failure-detection strategy for IGBT based on gate-voltage behavior applied to a motor drive system," *IEEE Trans. Ind. Electron.*, vol. 58, no. 5, pp. 1625–1633, May 2011.

[6] Y. Yang, Q. Zhang and P. Zhang, "A Fast IGBT Junction Temperature Estimation Approach Based on ON-State Voltage Drop," in *IEEE Trans. on Industry Applications*, vol. 57, no. 1, pp. 685-693, Jan.-Feb. 2021.

[7] Z. Hu, M. Du and K. Wei, "Online Calculation of the Increase in Thermal Resistance Caused by Solder Fatigue for IGBT Modules," in *IEEE Trans. on Device and Materials Reliability*, vol. 17, no. 4, pp. 785-794, 2017.

[8] H. Li, Y. Hu, S. Liu, Y. Li, X. Liao and Z. Liu, 'An Improved Thermal Network Model of the IGBT Module for Wind Power Converters Considering the Effects of Base-Plate Solder Fatigue', *IEEE Trans. on Device and Materials Reliability*, vol. 16, no. 4, pp. 570-575, 2016.

[9] A. S. Bahman, K. Ma, P. Ghimire, F. Iannuzzo and F. Blaabjerg, 'A 3-D-Lumped Thermal Network Model for Long-Term Load Profiles Analysis in High-Power IGBT Modules', *IEEE Journal of Emerging and Selected Topics in Power Electronics*, vol. 4, no. 3, pp. 1050-1063, 2016.

[10] B. Wang, J. Cai, X. Du and L. Zhou, "Review of power semiconductor device reliability for power converters," in *CPSS Transactions on Power Electronics and Applications*, vol. 2, no. 2, pp. 101-117, 2017.

[11] L. Dupont, Y. Avenas and P. Jeannin, "Comparison of Junction Temperature Evaluations in a Power IGBT Module Using an IR Camera and Three Thermo-sensitive Electrical Parameters," in *IEEE Transactions on Industry Applications*, vol. 49/4, pp. 1599-1608, 2013

[12] J. P. Bazzo, T. Lukasievicz, M. Vogt, et al., 'Thermal characteristics analysis of an IGBT using a Fiber Bragg Grating', *Opt. Laser Eng.*, vol. 50, no. 2, pp. 99-103, 2012.

[13] J.-L. Zhang, H. You, and F. Tian, "A fiber Bragg grating sensing system for monitoring IGBT temperature distribution and thermal conduction state of upper surface silicone," *Proc. SPIE*, vol. 10846, 2018, p. 1084616

[14] A. Mohammed et al., "Distributed Thermal Monitoring of Wind Turbine Power Electronic Modules Using FBG Sensing Technology," in *IEEE Sensors Journal*, vol. 20, no. 17, pp. 9886-9894, 1 Sept.1, 2020.

[15] S. Chen, D. Vilchis-Rodriguez, S. Djurović, M. Barnes, P. Mckeever and C. Jia, "Direct on Chip Thermal Measurement in IGBT Modules Using FBG Technology—Sensing Head Interfacing," in *IEEE Sensors Journal*, vol. 22, no. 2, pp. 1309-1320, 2022.

[16] A. Mohammed and S. Djurović, "A study of distributed embedded thermal monitoring in electric coils based on FBG sensor multiplexing," " Microprocessors and Microsystems, Elsevier, Volume 62, Pages 102-109, 2018.

[17] A. Mohammed, J. I. Melecio and S. Djurović, "Open-Circuit Fault Detection in Stranded PMSM Windings Using Embedded FBG Thermal Sensors," in *IEEE Sensors Journal*, vol. 19, no. 9, pp. 3358-3367, 2019.

[18] Y.-J. Rao, "In-fiber Bragg grating sensors," *Meas. Sci. Technol.*, vol. 8, no. 4, p. 355, 1997.

[19] D S Vilchis-Rodriguez, S Chen, S Djurović, M Barnes, P McKeever, C Jia, "IGBT Finite Element Model For Fiber Bragg Grating Sensor Installation Analysis", 11th Int. Conf. on Power Electronics Machines and Drives (IET PEMD 2022), Newcastle, UK, June 2022 (in press).

[20] S. Pangaro *et al.*, "Influence of fiber Bragg grating length on temperature measurements in laser-irradiated organs," *2016 IEEE International Symposium on Medical Measurements and Applications (MeMeA)*, 2016.